

# Electronic Structures, Spectroscopy, and Electrochemistry of $[\text{M}(\text{diimine})(\text{CN-BR}_3)_4]^{2-}$ ( $\text{M} = \text{Fe, Ru}$ ; $\text{R} = \text{Ph, C}_6\text{F}_5$ ) Complexes

Danh X. Ngo, Sarah A. Del Ciello, Alexandra T. Barth, Ryan G. Hadt, Robert H. Grubbs, Harry B. Gray\*, and Brendon J. McNicholas\*

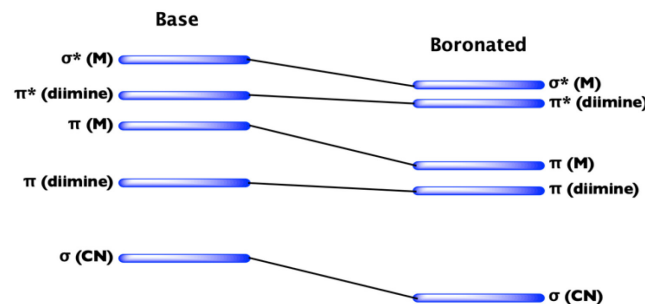
Beckman Institute, and Division of Chemistry and Chemical Engineering, California Institute of Technology, 1200 East California Boulevard, Mail Code 139-74, Pasadena, California 91125, United States

**ABSTRACT:** Complexes with the formula  $[\text{M}(\text{diimine})(\text{CN-BR}_3)_4]^{2-}$ , where diimine = bipyridine (bpy), phenanthroline (phen), 3,5-trifluoromethylbipyridine (flpy), R = Ph,  $\text{C}_6\text{F}_5$ , and M = Fe<sup>II</sup>, Ru<sup>II</sup> were synthesized and characterized by X-ray crystal structure analysis, UV-visible spectroscopy, IR spectroscopy, and voltammetry. Three highly soluble complexes,  $[\text{Fe}^{\text{II}}(\text{bpy})(\text{CN-B}(\text{C}_6\text{F}_5)_3)_4]^{2-}$ ,  $[\text{Ru}^{\text{II}}(\text{bpy})(\text{CN-B}(\text{C}_6\text{F}_5)_3)_4]^{2-}$ , and  $[\text{Ru}^{\text{II}}(\text{flpy})(\text{CN-B}(\text{C}_6\text{F}_5)_3)_4]^{2-}$  exhibit electrochemically reversible redox reactions, with large potential differences between the bpy<sup>0/−</sup> or flpy<sup>0/−</sup> and M<sup>III/II</sup> couples of 3.27, 3.52, and 3.19 V, respectively. CASSCF+NEVPT2 calculations accurately reproduce the effects of borane coordination on the electronic structures and spectra of cyanometallates.

Heteroleptic (diimine-cyanide) complexes of ruthenium,<sup>1</sup> iron,<sup>2</sup> copper,<sup>3</sup> iridium,<sup>4</sup> rhenium,<sup>5</sup> and osmium<sup>6,7</sup> have found use as vapochromic agents,<sup>8</sup> electrochemically reversible oxidants and reductants,<sup>7</sup> phosphors for organic light-emitting diodes,<sup>7,9,5</sup> and photooxidants and photoreductants.<sup>10</sup> We and others have shown that octahedral metal cyanides bond with boranes such as boron trifluoride, lowering the  $\sigma$  and  $\pi^*$  orbital energies of the cyanide ligand, which weakens metal–carbon bonding and strengthens CN bonding. Lowering the  $\pi^*$  cyanide orbitals enhances  $\pi$  backbonding, thereby increasing overall ligand field strengths.<sup>11,12,13</sup> Consequently, formal potentials for  $\text{M}^{(\text{n}+1)+}/\text{M}^{\text{n}+}$  couples are shifted anodically and metal-to-ligand charge transfer (MLCT) transitions are blue shifted, allowing resolution of ligand field (LF) absorptions, notably in hexacyanoferate(II).<sup>14</sup> Heteroleptic analogues, such as Os(bipyridine)<sub>2</sub>(CN-B(C<sub>6</sub>F<sub>5</sub>)<sub>3</sub>)<sub>2</sub>, also exhibit substantial anodic potential shifts for metal-centered redox events;<sup>7</sup> not surprising, shifts for diimine-localized redox processes are much smaller.<sup>7</sup> **Figure 1** depicts the general changes in one-electron energy levels that occur upon boronation of a heteroleptic tetracyanometallate that possesses an aromatic ligand.

Earlier we reported that coordination of tris(pentafluorophenyl)borane (BCF) to  $[\text{Fe}(\text{CN})_6]^{4-}$  anodically shifts the formal Fe<sup>III/II</sup> potential by over 2.1 V.<sup>14</sup> Since complexes with two differently tunable redox centers are relatively rare, we have extended our investigations of boronated cyanometallates to include heteroleptic complexes containing 2,2'-bipyridine (bpy), 3,5-trifluoromethylbipyridine (flpy), or phenanthroline (phen). Boronation with BPh<sub>3</sub> or BCF afforded  $[\text{M}(\text{diimine})(\text{CN-BR}_3)_4]^{2-}$  (M = Fe<sup>II</sup>, Ru<sup>II</sup>; diimine = bpy, phen, flpy; and R = Ph, C<sub>6</sub>F<sub>5</sub>) derivatives. In addition to their utility as chromophores,<sup>10,15,16,17</sup> these complexes possess impressive electrochemical properties. To enhance our understanding of the effects of boronation on MLCT transitions, we performed *ab initio* calculations on trihydridoborane analogues of the heterolep-

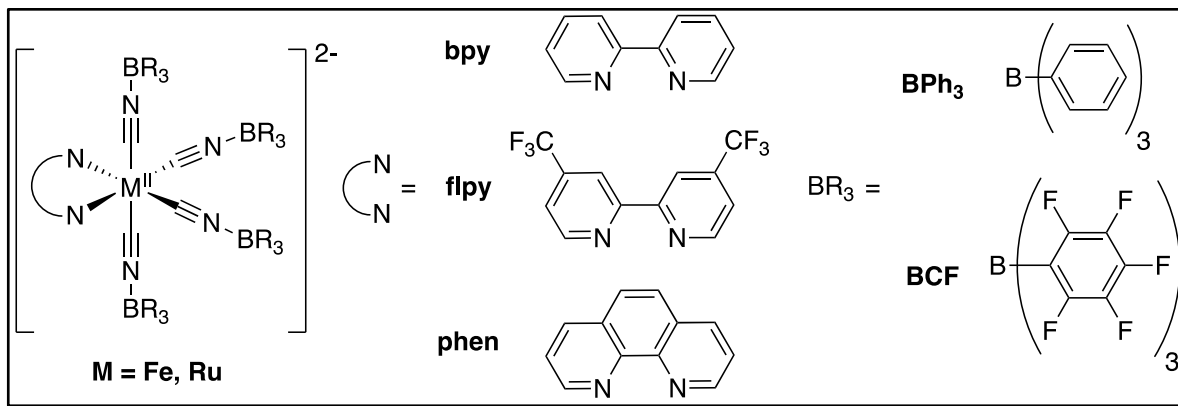
tic cyanometallates using the complete active space self-consistent field (CASSCF) method coupled with n-electron valence state second-order perturbation theory (NEVPT2). Our calculations demonstrate the accuracy of CASSCF+NEVPT2 for both LF and MLCT states of boronated cyanoruthenates. We also probed the excited-state properties of Fe<sup>II</sup> analogues, as we hoped boronation would extend the lifetimes of these typically short-lived states.



**Figure 1.** One-electron energy level changes resulting from boronation of  $[\text{M}(\text{diimine})(\text{CN})_4]^{2-}$ .

## Synthesis and X-ray Crystallography:

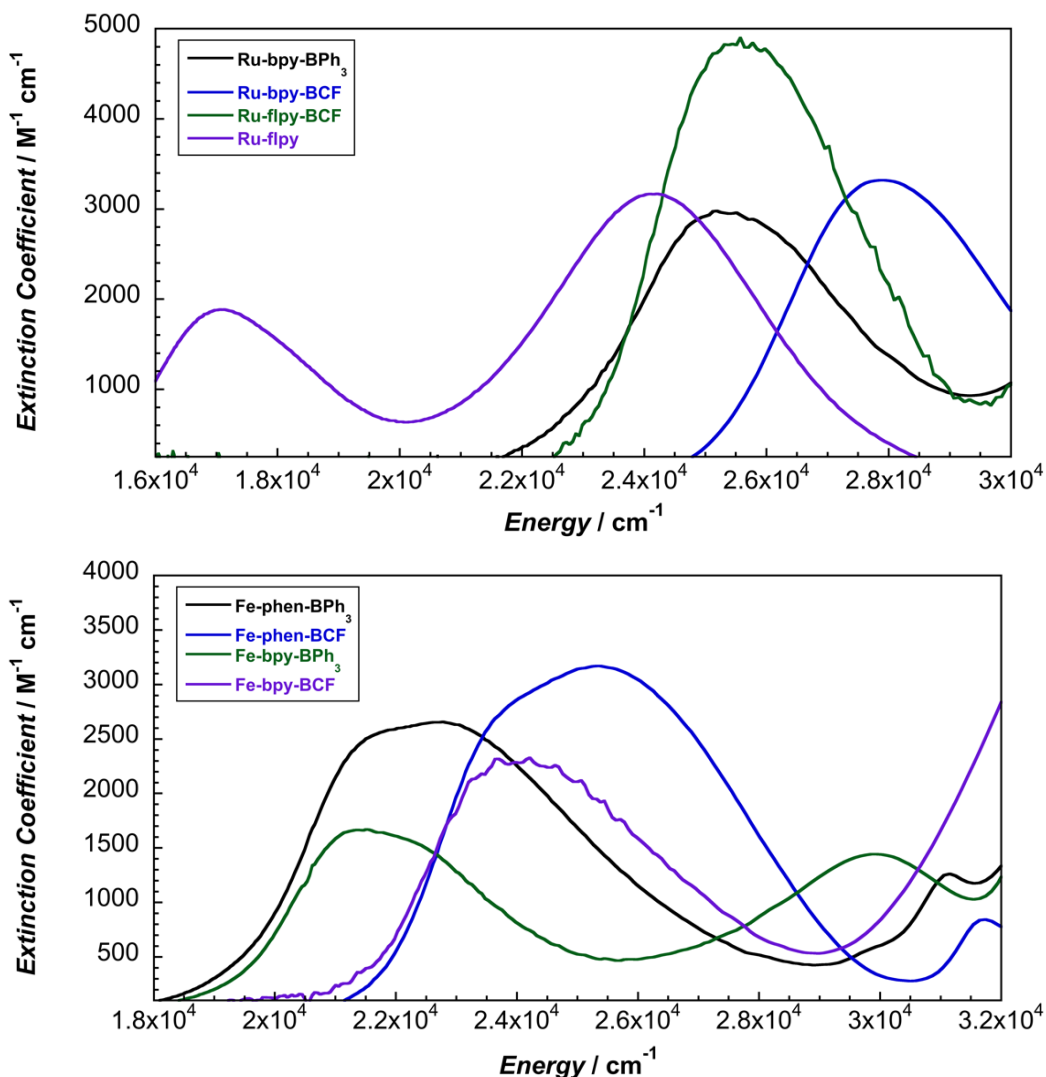
The potassium salts of the precursor  $[\text{M}^{\text{II}}(\text{diimine})(\text{CN})_4]^{2-}$ -complexes were synthesized according to literature methods.<sup>18,19</sup>  $\text{K}_2[\text{Ru}(\text{flpy})(\text{CN})_4]$  (**Ru-flpy**) was prepared in a similar manner. Bis(triphenylphosphine)iminium ( $\text{PPN}^+$ ) salts of the anions were obtained by addition of a stoichiometric excess of  $\text{PPNCl}$  to an aqueous solution of  $\text{K}_2[\text{M}^{\text{II}}(\text{diimine})(\text{CN})_4]$ , yielding a solid that was collected by filtration. The tetrabutylammonium ( $\text{TBA}^+$ ) salts of selected anions were prepared through metathesis with hydrochloric acid to precipitate  $\text{H}_2[\text{M}^{\text{II}}(\text{diimine})(\text{CN})_4]$ . Subsequent titration with  $\text{TBAOH}$  afforded  $(\text{TBA})_2[\text{M}^{\text{II}}(\text{diimine})(\text{CN})_4]$ .



**Figure 2.** Structures of  $[M(\text{diimine})(\text{CN-BR}_3)_4]^{2-}$ , diimine ligands, and boranes investigated in this work.

To obtain the borane adducts of these species, a slight excess of BPh<sub>3</sub> or BCF was added to a nitrogen-purged dichloromethane solution of the TBA<sup>+</sup> or PPN<sup>+</sup> salts of  $[\text{M}^{\text{II}}(\text{diimine})(\text{CN})_4]^{2-}$  complexes under reflux conditions. Addition of hexanes (excess) to a concentrated solution afforded the following complexes:  $(\text{TBA})_2[\text{Fe}^{\text{II}}(\text{bpy})(\text{CN-BPh}_3)_4]$  (**Fe-bpy-BPh<sub>3</sub>**),  $(\text{TBA})_2[\text{Fe}^{\text{II}}(\text{bpy})(\text{CN-B}(\text{C}_6\text{F}_5)_3)_4]$  (**Fe-bpy-BCF**),  $(\text{TBA})_2[\text{Fe}^{\text{II}}(\text{phen})(\text{CN-BPh}_3)_4]$  (**Fe-phen-BPh<sub>3</sub>**),  $(\text{TBA})_2[\text{Fe}^{\text{II}}(\text{phen})(\text{CN-B}(\text{C}_6\text{F}_5)_3)_4]$  (**Fe-phen-BCF**),

$(\text{TBA})_2[\text{Ru}^{\text{II}}(\text{bpy})(\text{CN-BPh}_3)_4]$  (**Ru-bpy-BPh<sub>3</sub>**),  $(\text{TBA})_2[\text{Ru}^{\text{II}}(\text{bpy})(\text{CN-B}(\text{C}_6\text{F}_5)_3)_4]$  (**Ru-bpy-BCF**), and  $(\text{PPN})_2[\text{Ru}(\text{flpy})(\text{CN-B}(\text{C}_6\text{F}_5)_3)_4]$  (**Ru-flpy-BCF**). Characterization by <sup>1</sup>H NMR, <sup>11</sup>B NMR and, when applicable, <sup>19</sup>F NMR, confirmed that all compounds were pure. All compounds also were characterized by elemental analysis or mass spectrometry, IR spectroscopy, voltammetry, and UV-visible spectroscopy. **Figure 2** provides structural representations of the complexes investigated in this work.



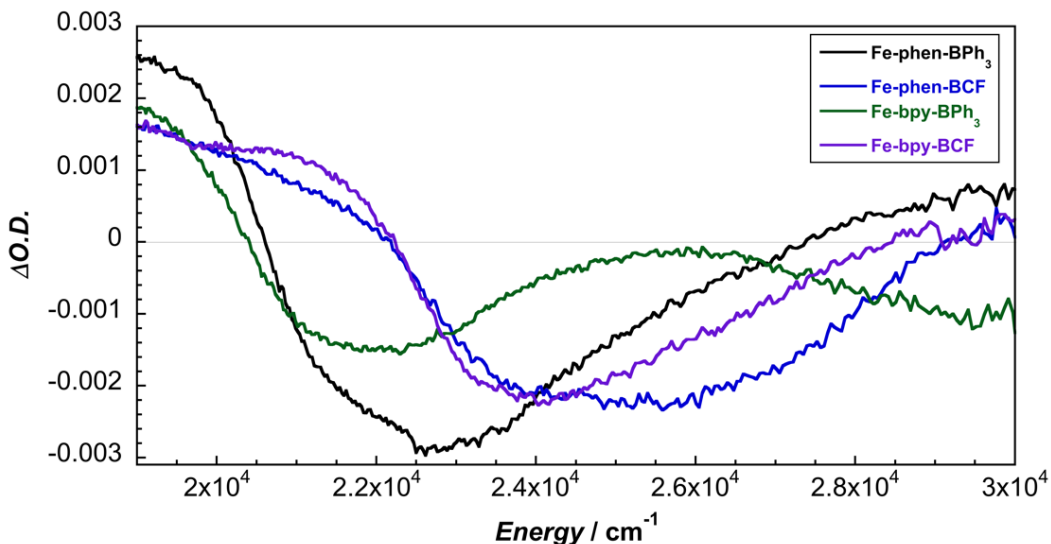


**Figure 3. (Top)** UV-visible absorption spectra of  $[\text{Ru}(\text{diimine})(\text{CN})_4]^{2-}$ ; **(Middle)**  $[\text{Fe}(\text{diimine})(\text{CN-BR}_3)_4]^{2-}$  in MeCN solution; **(Bottom)** transient absorption spectra of  $[\text{Fe}(\text{diimine})(\text{CN-BR}_3)_4]^{2-}$  in MeCN solution obtained 1 ps after  $34,500 \text{ cm}^{-1}$  (290 nm) excitation.

Growth of X-ray quality crystals proved challenging for these complexes due to their tendency to form oils. However, we were able to obtain four crystal structures: **Ru-flyp**, **Ru-flyp-BCF**, consistent with a slight decrease in  $\pi$  back donation due to electron withdrawal by the flyp trifluoromethyl groups. NMR and IR spectra are shown in the supporting information (Figures S1-S31).

**Table 1.** Vibrational and metal-to-ligand charge transfer data for  $[\text{M}(\text{diimine})(\text{CN})_4]^{2-}$  and  $[\text{M}(\text{diimine})(\text{CN-BR}_3)_4]^{2-}$  in MeCN.

Species	$\nu_{\text{CN}} (\text{cm}^{-1})$	$\lambda_{\text{MLCT}} (\text{nm})$	$\epsilon (\text{M}^{-1} \text{ cm}^{-1})$
Fe-bpy <sup>a,b</sup>	2047, 2077	654, 440	---
Fe-bpy-BPh <sub>3</sub>	2145, 2181	465, 333	1670, 1940
Fe-bpy-BCF	2170, 2207	413, 309	2360, 4170
Fe-phen	2045, 2074	615	---
Fe-phen-BPh <sub>3</sub>	2146, 2182	439	2610
Fe-phen-BCF	2169, 2206	394	3160
Ru-bpy <sup>c</sup>	2051, 2082	535, 374	---
Ru-bpy-BPh <sub>3</sub>	2140, 2188	397, 309	2950, 5000
Ru-bpy-BCF	2168, 2216	350	3000
Ru-flyp	2062, 2090	584, 413	3850, 6130
Ru-flyp-BCF	2171, 2218	392, 320	3830, 4560

<sup>a</sup>Reference 20. <sup>b</sup>Reference 21. <sup>c</sup>Reference 22.

**BCF, Fe-phen-BPh<sub>3</sub>, and Fe-phen-BCF.** Comparing **Ru-flyp** and **Ru-flyp-BCF**, there is a negligible change in the average C-N bond length and a minor shortening (ca. 0.05 Å) of the average Ru-C bond length. These small structural changes are consistent with work on boronated hexacyanoferrates.<sup>14</sup>

#### Infrared and UV-visible Spectroscopy:

IR stretching frequencies, MLCT absorbance maxima (and extinction coefficients) for the parent complexes and heteroleptic isocyanoborates are set out in **Table 1**. Only one MLCT transition is reported for **Fe-phen-BCF** and **Fe-phen-BPh<sub>3</sub>** due to overlap with the first  $\pi-\pi^*$  absorption of the phenanthroline ligand. The blueshifts in CN stretching frequencies indicate strengthening of the CN bond due to coordination of borane to the nitrogen lone pair.<sup>11,23</sup> The IR stretching frequencies for **Ru-flyp-BCF** are very slightly blueshifted from those of **Ru-bpy**.

**BCF**, consistent with a slight decrease in  $\pi$  back donation due to electron withdrawal by the flyp trifluoromethyl groups. NMR and IR spectra are shown in the supporting information (Figures S1-S31).

**Figure 3** displays UV-vis spectra for all newly reported species. It is well known that Fe and Ru diimine complexes exhibit two well-defined MLCT absorption maxima in the visible/near-UV region that are strongly solvatochromic.<sup>24</sup> For example, the **Ru-flyp** MLCT absorptions red shift by 5500  $\text{cm}^{-1}$  when the solvent is changed from water to acetonitrile.<sup>25</sup> This shift is expected in view of the much larger Gutmann-Beckett acceptor number of  $\text{H}_2\text{O}$  compared to MeCN.<sup>26</sup> In contrast to the dramatic shifts observed in MLCT transitions, the  $\pi-\pi^*$  absorption shifts only slightly (550  $\text{cm}^{-1}$ ), indicating that solvent interactions and, by extension MCN-B bonding, minimally perturb diimine orbital energies.

MLCT bands in BCF adducts are blueshifted more than those reported for  $\text{Fe}(\text{bpy})_2(\text{CN-BPh}_3)$  and  $\text{Os}(\text{bpy})_2(\text{CN-BPh}_3)_2$ ,<sup>7,27</sup> likely due to the greater ligand field stabilization of occupied d orbitals upon boronation of the tetracyano complexes.<sup>2</sup> The flyp trifluoromethyl substituents inductively withdraw electron density, redshifting MLCT transitions, while boronation blue shifts them.<sup>25</sup> Additionally, BCF steric hindrance attenuates the MLCT energy dependence on solvent. Interestingly, the lowest energy MLCT transition linearly correlates with the difference between the formal potentials for one-electron oxidations and reductions, as shown in **Figure 4** for ruthenium-based compounds. As the process is electrochemically irreversible, the **Ru-bpy-BPh<sub>3</sub>** formal potential was estimated from the inflection potential of a 100  $\text{mV s}^{-1}$  cyclic voltammogram.<sup>28</sup>

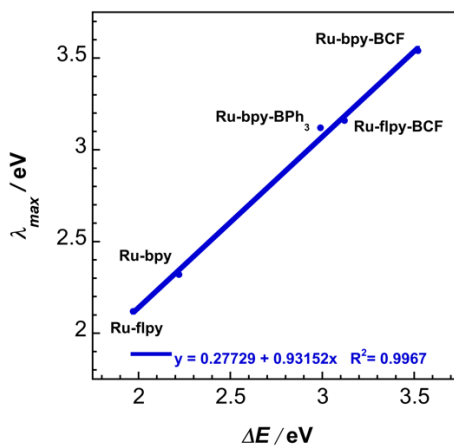


**Figure 4.** MLCT absorbance maximum versus difference in formal potential for heteroleptic ruthenium complexes. All spectra and voltammetry acquired in MeCN.

#### Transient Absorption Spectroscopy:

Excited-state lifetimes of **Fe-bpy-BPh<sub>3</sub>**, **Fe-phen-BPh<sub>3</sub>**, **Fe-bpy-BCF**, and **Fe-phen-BCF** were investigated using ultrafast transient absorption (TA) spectroscopy. 0.33–0.35 mM samples in MeCN were prepared under a N<sub>2</sub> atmosphere. A 2 mm path length cuvette was used for all spectra, which corresponds to approximately 1 a.u. optical density at the excitation wavelength. The differential absorption spectra of the four Fe complexes obtained 1 ps after excitation are shown in the bottom panel of **Figure 3**. Each complex displays concomitant ground state bleach (GSB) and excited-state absorption (ESA) features upon irradiation, with **Fe-bpy-BCF** and **Fe-phen-BCF** exhibiting a ~1500 cm<sup>-1</sup> blueshift in isosbestic point versus **Fe-bpy-BPh<sub>3</sub>** and **Fe-phen-BPh<sub>3</sub>** (**Figures S45** and **S49** versus **Figures S43** and **S47**). A sharp ESA feature at 27,000/24,000 cm<sup>-1</sup> and a broad GSB system at 19,000/16,000 cm<sup>-1</sup> corresponding to the bpy/phen radical anion were not observed, suggesting that the transient feature before relaxation is not attributable to a charge transfer state.<sup>29,30</sup> Instead, the spectral features likely originate from a LF state that preferentially forms due to the high energy of the MLCT state. The excited-state kinetics and spectral features for these species are consistent with those previously assigned as LF (<sup>3</sup>MC or <sup>5</sup>MC) in related work on **Fe-bpy** in coordinating solvents.<sup>2,31,32</sup> The ESA observed around 20,000/22,000 cm<sup>-1</sup> supports this interpretation, since the absorption likely is due to a lower energy MLCT transition coming from a relaxed LF excited state.<sup>20</sup>

As a control, we also measured the TA spectrum of **Fe-phen** in MeCN. Previous studies on **Fe-bpy** in solvents with low Gutmann-Beckett acceptor numbers (AN = 19.3 for MeCN; AN = 19.3 for dimethyl sulfoxide; AN = 12.5 for acetone)<sup>33</sup> demonstrated that the **Fe-bpy** MLCT is much longer-lived (picoseconds versus hundreds of femtoseconds)<sup>2,20,32</sup>. Consistent with these studies, the TA spectrum for **Fe-phen** displays a sharp ESA around 27,000 cm<sup>-1</sup> and a broad GSB around 17,000 cm<sup>-1</sup>, corresponding to population of a transient MLCT state involving phenanthroline that preferentially forms over the MC transient state (**Figure S41**).

While excited-state lifetimes for BPh<sub>3</sub> adducts are virtually identical with those of the parents, both **Fe-bpy-BCF** (22.4 ± 2.3 ps) and **Fe-phen-BCF** (25.1 ± 2.3 ps) exhibit slight increases, presumably due to diminished solvent-based non-radi-

ative decay pathways.<sup>25</sup> **Table S1** lists all excited-state lifetimes; **Figures S41–S55** provide additional time-dependent TA data and first-order exponential decay fits.

#### Density Functional Theory (DFT) and CASSCF+NEVPT2 Calculations:

Optimizations and CASSCF+NEVPT2 calculations were performed for the heteroleptic cyanoruthenates. Previous *ab initio* theoretical work on both homoleptic and heteroleptic cyanometallates predicted both LF and charge transfer transitions with high accuracy, provided an appropriate active space was chosen.<sup>34,35,36</sup>

In calculations of the boronated complexes, trihydridoborane (BH<sub>3</sub>) was used as a mimic for BCF to decrease computational cost; arguably, the results should be valid, as the two boranes are both strong Lewis acids [Gutmann-Beckett acceptor numbers: BH<sub>3</sub> (75.8); BCF (78.9)].<sup>37</sup>

All calculations were performed in ORCA 4.2.1.<sup>38</sup> All DFT structural optimizations used the PBE0 functional, the def2-QZVPP basis set for Ru, and the def2-TZVP basis set for all other atoms. The conductor-like polarizable continuum model (CPCM) was used to account for solvation in acetonitrile ( $\epsilon = 36.64$ ). X-ray crystal structures of **Ru-fipy**, **Ru-bpy** and **Ru-fipy-BCF** were used as initial guesses for structural optimization. X-ray crystal structure bond lengths along with those obtained from ground-state optimizations are set out in **Table 2**. In all cases, the bond lengths obtained from theory are in good agreement with those obtained from X-ray crystallography.

All CASSCF calculations were state averaged, with one quintet, nine triplets, and ten singlets included. The coordinates of all complexes were aligned such that the dimine ligand was coincident with the *xy* plane. For all complexes, the active space consisted of three metal t<sub>2g</sub>  $\pi$ -bonding orbitals, two metal  $\sigma^*$  orbitals, two CN  $\sigma$  bonding orbitals, three CN  $\pi^*$  + Ru 5d orbitals, one diimine  $\pi$  orbital, and two diimine  $\pi^*$  orbitals, giving twelve electrons in thirteen orbitals (CAS(12,13)). **Figure 5** depicts the active space orbitals for **Ru-fipy**. We reduced the number of  $\pi$  bonding orbitals given the negligible change in

**Table 2.** Experimental and DFT-optimized bond lengths for heteroleptic cyanometallates.

Bond / Length (Optimized/Experimental)	Ru-flpy (Å)	Ru-flpy-BCF (Å)	Ru-bpy <sup>a</sup>
<b>M-CN (Axial)</b>	1.9705 / 2.0090(19)	2.0114 / 2.0167(16)	2.0268 / 2.070
<b>M-CN (Axial)</b>	2.0294 / 2.063(2)	2.0112 / 2.0137(16)	2.02683 / 2.063
<b>M-CN (Equatorial)</b>	1.9707 / 2.017(2)	1.9537 / 1.9687(16)	1.96714 / 2.011
<b>M-CN (Equatorial)</b>	2.0296 / 2.059(2)	1.9537 / 1.9640(16)	1.96676 / 1.989
<b>M-N<sub>1</sub></b>	2.1024 / 2.0880(15)	2.1141 / 2.1052(14)	2.11414 / 2.115
<b>M-N<sub>2</sub></b>	2.1024 / 2.0816(16)	2.1143 / 2.1043(14)	2.11434 / 2.100
<b>C≡N<sub>1</sub></b>	1.1683 / 1.160(3)	1.1575 / 1.1494(19)	1.16946 / 1.128
<b>C≡N<sub>2</sub></b>	1.1683 / 1.161(3)	1.1593 / 1.155(2)	1.16943 / 1.162
<b>C≡N<sub>3</sub></b>	1.1664 / 1.158(3)	1.1593 / 1.1553(19)	1.16724 / 1.125
<b>C≡N<sub>4</sub></b>	1.1663 / 1.162(3)	1.1575 / 1.150(2)	1.16728 / 1.139

<sup>a</sup>Reference 8

MLCT transition energies that resulted from inclusion of the HOMO – 1 for bpy or flpy. NEVPT2 was used to account for dynamical correlation of active-space electrons.<sup>35</sup> DFT optimization input files and the active space orbital depictions for **Ru-flpy**, **Ru-bpy-BCF**, and **Ru-flpy-BCF** are given in the supporting information (Figures S71-S73).

Calculated energies of MLCT and LF transitions for heteroleptic cyanoruthenates are given in **Table 3** and **Table 4**, respectively. The calculations for all four complexes are in excellent agreement with the two experimental MLCT maxima for each species, with higher MLCT energies for both boronated complexes and higher MLCT energies for **Ru-bpy-BH<sub>3</sub>** compared to **Ru-flpy-BH<sub>3</sub>**.

CASSCF+NEVPT2 also correctly predicts moderate blueshifts of LF excited states upon boronation of ruthenates. We therefore suggest that the Gutmann-Beckett acceptor number is a useful parameter in estimating the relative excited-state energies of boronated complexes.<sup>39</sup>

**Table 3** Experimental and calculated singlet MLCT transition energies for heteroleptic cyanoruthenates.

Complex	Orbital Transition	MLCT Energy, Experimental (cm <sup>-1</sup> )	MLCT Energy, NEVPT2 (cm <sup>-1</sup> )	Oscillator Strength
<b>Ru-bpy</b>	$d_{yz} \rightarrow \pi^*_1$	---	16,870	0.00126
	$d_{x^2-y^2} \rightarrow \pi^*_1$	---	17,540	0.0000155
	$d_{xz} \rightarrow \pi^*_1$	18,690	19,150	0.231
	$d_{yz} \rightarrow \pi^*_2$	---	23,880	0.00925
	$d_{x^2-y^2} \rightarrow \pi^*_2$	---	24,530	0.0000379
	$d_{xz} \rightarrow \pi^*_2$	26,738	25,620	0.0848
<b>Ru-fipy</b>	$d_{yz} \rightarrow \pi^*_1$	---	14,490	0.00197
	$d_{x^2-y^2} \rightarrow \pi^*_1$	---	15,230	0.0000276
	$d_{xz} \rightarrow \pi^*_1$	17,120	17,550	0.271
	$d_{yz} \rightarrow \pi^*_2$	---	21,950	0.00802
	$d_{x^2-y^2} \rightarrow \pi^*_2$	---	22,680	0.0000239
	$d_{xz} \rightarrow \pi^*_2$	24,210	23,810	0.0819
<b>Ru-bpy-BH<sub>3</sub></b>	$d_{yz} \rightarrow \pi^*_1$	---	23,940	0.000245
	$d_{x^2-y^2} \rightarrow \pi^*_1$	---	24,420	0.00000899
	$d_{xz} \rightarrow \pi^*_1$	28,570	25,720	0.204
	$d_{yz} \rightarrow \pi^*_2$	---	31,290	0.0113
	$d_{x^2-y^2} \rightarrow \pi^*_2$	---	31,840	0.0000831
	$d_{xz} \rightarrow \pi^*_2$	---	32,700	0.0624
<b>Ru-fipy-BH<sub>3</sub></b>	$d_{yz} \rightarrow \pi^*_1$	---	21,150	0.00113
	$d_{x^2-y^2} \rightarrow \pi^*_1$	---	21,640	0.0000139
	$d_{xz} \rightarrow \pi^*_1$	25,510	23,240	0.238
	$d_{yz} \rightarrow \pi^*_2$	---	29,020	0.00927
	$d_{x^2-y^2} \rightarrow \pi^*_2$	---	29,600	0.0000517
	$d_{xz} \rightarrow \pi^*_2$	31,250	30,500	0.0579

**Table 4.** Calculated singlet LF transition energies for heteroleptic cyanoruthenates.

Complex	Orbital Transition	Transition Energy, NEVPT2 (cm <sup>-1</sup> )	Oscillator Strength
<b>Ru-bpy</b>	$d_{x^2-y^2} \rightarrow d_{xy}$	39,210	0.00313
	$d_{yz} \rightarrow d_{xy}$	42,270	0.00954
	$d_{xz} \rightarrow d_{xy}$	43,480	0.0000112
<b>Ru-fipy</b>	$d_{x^2-y^2} \rightarrow d_{xy}$	39,580	0.00272
	$d_{yz} \rightarrow d_{xy}$	42,700	0.00893
	$d_{xz} \rightarrow d_{xy}$	44,160	0.00000423
<b>Ru-bpy-BH<sub>3</sub></b>	$d_{x^2-y^2} \rightarrow d_{xy}$	42,990	0.00381
	$d_{yz} \rightarrow d_{xy}$	47,600	0.0132
	$d_{xz} \rightarrow d_{xy}$	48,250	0.00000160
<b>Ru-fipy-BH<sub>3</sub></b>	$d_{x^2-y^2} \rightarrow d_{xy}$	40,470	0.00290
	$d_{yz} \rightarrow d_{xy}$	43,590	0.0119
	$d_{xz} \rightarrow d_{xy}$	44,570	0.0000131

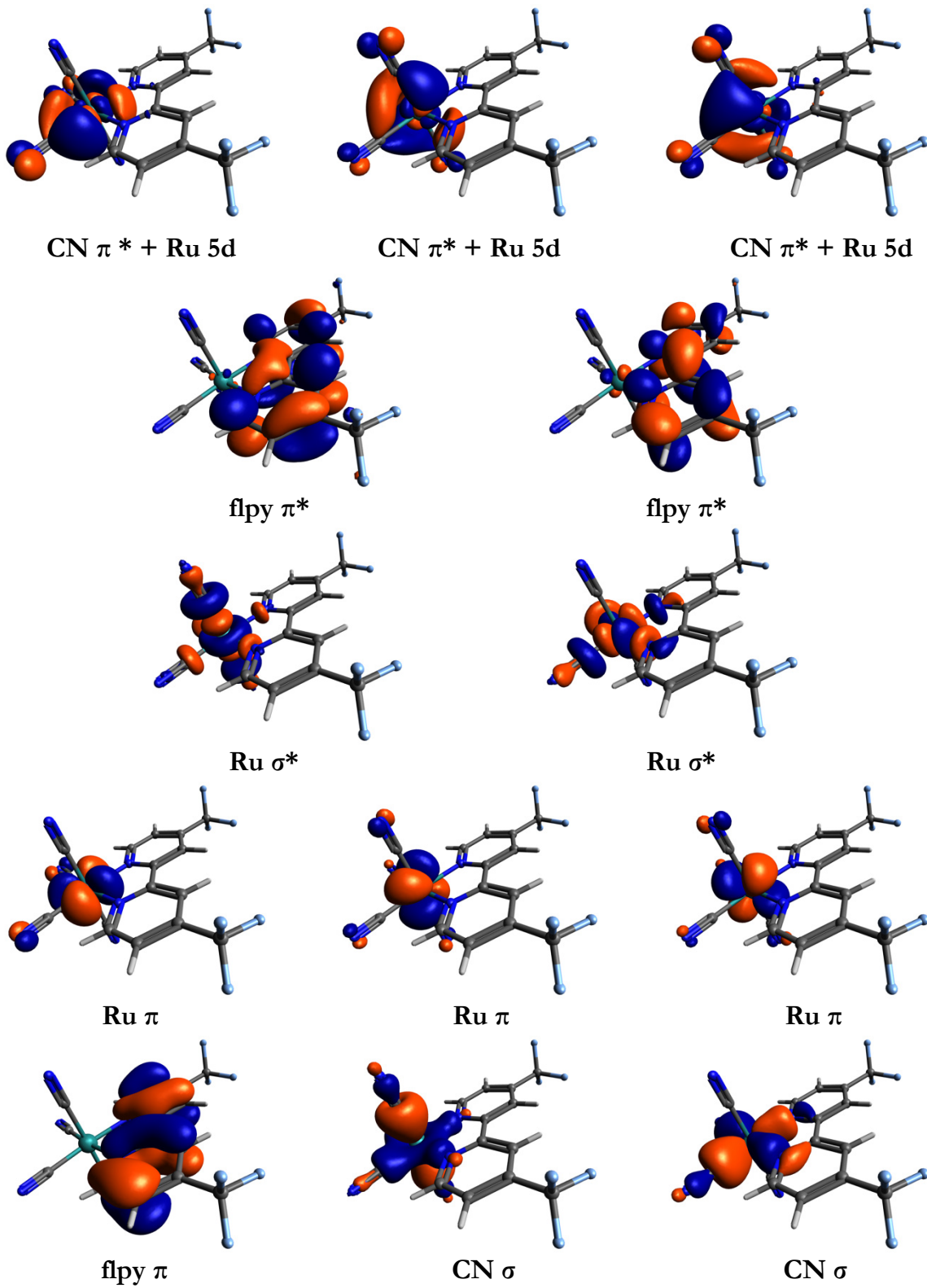


**Figure 5.** Active space molecular orbitals for state-averaged CAS(12,13) of  $[\text{Ru}(\text{fipy})(\text{CN})_4]^{2-}$ . Isosurface values set to 0.04.

#### Electrochemistry:

Formal potentials (or peak potentials in electrochemically irreversible cases), peak current ratios ( $i_{\text{p,a}}/i_{\text{p,c}}$ ), and diffusion coefficients ( $D_0$ ) are summarized in **Table 5**. **Figure 6** displays the voltammetry of five heteroleptic tetracyanometallates.

Diffusion coefficients were calculated from linear fits of peak current versus the square root of the scan rate (Randles-Sevcik equation):

$$i_p = 0.4463 C_0 n F A \left( \frac{n F v D}{R T} \right)^{1/2}$$

Where  $C_0$  is the bulk concentration of redox active species,  $n$  is the number of electrons transferred in each redox process (one in this case),  $F$  is Faraday's constant,  $A$  is the surface area of the electrode,  $v$  is the scan rate,  $R$  is the ideal gas constant, and  $T$  is the temperature.<sup>40</sup> All complexes exhibit diffusion coefficients on the order of  $10^{-6} \text{ cm}^2 \text{ s}^{-1}$ , suggesting that boronation does not significantly affect the diffusional properties of these complexes. We note that most of the boronated species exhibit somewhat smaller diffusion coefficients compared to the bare species, as expected from viscoelastic considerations, though the minimal decrease is likely a result of differences in ion-pairing or solvent interactions between bare versus boronated species.

Given the anodic formal potentials for these species, peak current ratios were calculated using an empirical formula that deconvolutes the current at the reversal potential from the redox event

$$\frac{i_{p,c}}{i_{p,a}} = \frac{i_{p,c,0}}{i_{p,a,0}} + \frac{i_{p,c,0}}{i_{sp}} + 0.0486$$

where  $i_{p,c}/i_{p,a}$  is the corrected peak current ratio,  $i_{p,c,0}/i_{p,a,0}$  is the peak current ratio relative to zero current, and  $i_{p,c,0}/i_{sp}$  is

the ratio of the uncorrected peak cathodic current and the current at the switching potential.<sup>41</sup>

Cyclic voltammetry curves for all parent complexes and their tris(pentafluorophenyl)borane adducts confirm that electron transfer is nearly or fully reversible for both ligand-centered reductions and metal-centered oxidations. Bare bipyridine complexes are reduced through an ECE mechanism, where electron transfer results in bipyridine dissociation followed by additional reduction.<sup>42</sup> In contrast, decomposition was not observed for reduction of all BCF and BPh<sub>3</sub> adducts. This behavior likely results from the slight anodic shift in potential for diimine reduction, suggesting that the diimine radical is stable on the time scale of voltammetry.

Interestingly, previous work demonstrated that  $[\text{Fe}(\text{CN}-\text{BPh}_3)_6]^{4-}$  oxidation is electrochemically irreversible.<sup>14</sup> As evidenced from both chemical and electrochemical experiments, oxidation results in dissociation of one or more boranes. Consistent with these results, the BPh<sub>3</sub> adducts of heteroleptic complexes exhibited similar anodic responses. As a side note, the smaller peak current ratio for **Ru-fipy-BCF** oxidation in MeCN could be due to the redox event being too close to the MeCN solvent window.

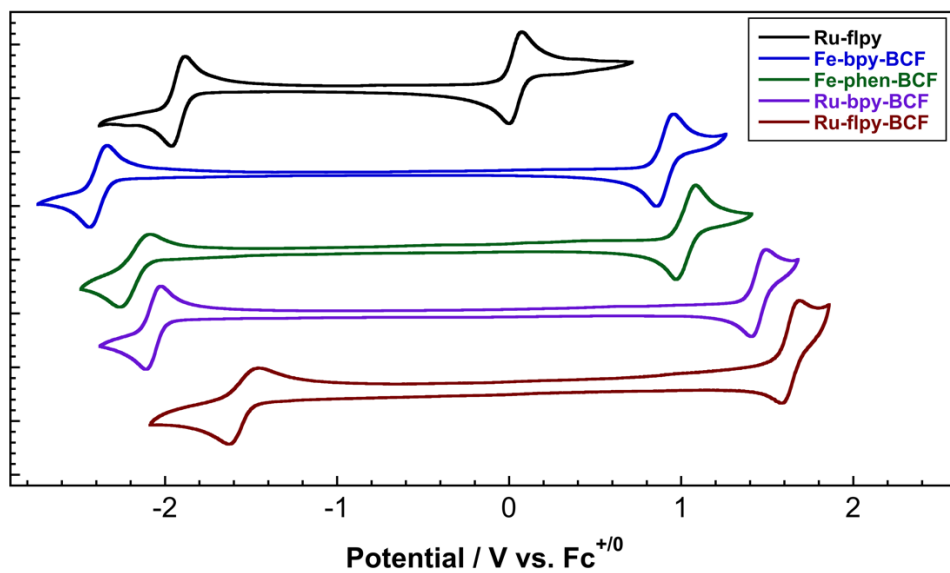


**Figure 6.** Voltammetry of parent and boronated  $[\text{M}(\text{diimine})(\text{CN})_4]^{2-}$  complexes. Voltammetry of **Fe-bpy-BCF** was acquired in THF. All other voltammetry was acquired in MeCN. Supporting electrolyte was 0.1-0.2 M TBAPF<sub>6</sub> with electronic compensation for 85% of the uncompensated resistance. All potentials referenced to Fc<sup>+/-</sup>.

**Table 5.** Electrochemical data for  $[M(\text{diimine})(\text{CN})_4]^{2-}$  and  $[M(\text{diimine})(\text{CN-BR}_3)_4]^{2-}$ . Formal potentials or peak potentials, potential separations, and peak current ratios are for 100 mV s<sup>-1</sup> scan rates (0.1 - 0.2 M TBAPF<sub>6</sub> electrolyte).

Solvent	Species	$E^{\text{III/II}}(\text{V vs. Fc}^{+/\text{0}})$	$E^{\text{0/-}}(\text{V vs. Fc}^{+/\text{0}})$	$\Delta E_{\text{ox}}(\text{mV})$	$\Delta E_{\text{red}}(\text{mV})$	$i_{\text{p,a}}/i_{\text{p,c}}(\text{ox})$	$i_{\text{p,a}}/i_{\text{p,c}}(\text{red})$	$D_0(\text{cm}^2 \text{ s}^{-1})$
MeCN	Fe-bpy	-0.64	-2.54 <sup>b</sup>	76	---	0.99	---	$5.9 \times 10^{-6}$ (ox.)
	Fe-bpy-BPh <sub>3</sub>	0.66 <sup>a</sup>	-2.19	---	95	---	0.98	$4.8 \times 10^{-6}$ (red.)
	Fe-bpy-BCF	1.00	-2.17	87	110	1.04	0.84	---
	Fe-phen	-0.62	-2.46	75	88	0.99	0.73	$8.2 \times 10^{-6}$ (ox.); $5.8 \times 10^{-6}$ (red.)
	Fe-phen-BPh <sub>3</sub>	0.43 <sup>a</sup>	-2.11	---	290	---	1.05	---
	Fe-phen-BCF	1.02	-2.17	87	97	0.99	0.70	$4.7 \times 10^{-6}$ (ox.); $5.1 \times 10^{-6}$ (red.)
	Ru-bpy	-0.17	-2.39	80	80	1.01	0.72	$2.6 \times 10^{-6}$ (ox.)
	Ru-bpy-BPh <sub>3</sub>	0.90 <sup>a</sup>	-2.13	---	100	---	0.92	$2.1 \times 10^{-6}$ (red.)
	Ru-bpy-BCF	1.43	-2.09	85	85	1.00	1.00	$5.0 \times 10^{-6}$ (ox.); $4.2 \times 10^{-6}$ (red.)
	Ru-fipy	0.05	-1.92	76	84	0.94	0.93	$5.2 \times 10^{-6}$ (ox.); $6.1 \times 10^{-6}$ (red.)
	Ru-fipy-BCF	1.63	-1.56	95	115	0.75	0.97	$7.4 \times 10^{-6}$ (ox.); $2.2 \times 10^{-6}$ (red.)
THF	Fe-bpy-BCF	0.91	-2.36	100	100	1.00	0.99	$2.9 \times 10^{-6}$ (ox.); $2.8 \times 10^{-6}$ (red.)

<sup>a</sup>Peak anodic potential. <sup>b</sup>Peak cathodic potential

The separations in formal potentials for these species are among the highest ever reported.<sup>1,15</sup> To our knowledge, only heteroleptic species with alkyl isocyanides exhibit greater formal potential separations (the separation for  $[\text{Ru}(\text{bpy})(\text{CN-Me})_4]^{2+}$  is 3.70 V).<sup>15</sup> As two of the boronated complexes have greatly separated potentials [**Ru-fipy-BCF** (3.19 V); **Ru-bpy-BCF** (3.52 V)] and long excited-state lifetimes, they likely will be useful photooxidants and photoreductants (see Figure 7 for excited-state potentials of **Ru-fipy-BCF** and **Ru-bpy-BCF**. The  $[\text{Ru}(\text{bpz})_3]^{2+}$  excited-state potential (1.07 V vs. Fc<sup>+/\text{0}</sup>) is comparable to that of **Ru-fipy-BCF**).<sup>25,43,44</sup>

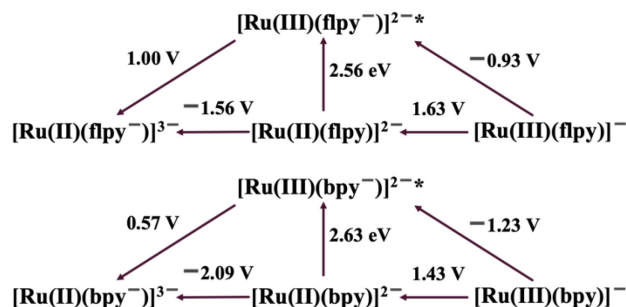


**Figure 7.** Modified Latimer diagrams: **Ru-fipy-BCF** (upper); **Ru-bpy-BCF** (lower). Potentials vs Fc<sup>+/\text{0}</sup>.

### Concluding Remarks:

We have extended investigations of boronated cyanometalates to include heteroleptic species with a variety of diimine ligands. We demonstrated that the formal potentials of heteroleptic iron and ruthenium complexes can be tuned with boranes while preserving or improving the solubilities, stabilities, and

electronic properties. Importantly, we have shed new light on the factors that control Lewis-acid-tuning of both formal potentials and MLCT energies using both experimental and theoretical studies, which should aid the development of vapochromic sensors, photoredox catalysts, and electrolytes for symmetric, non-aqueous redox flow batteries.<sup>45</sup>

### Experimental:

#### General

$\text{K}_2[\text{Fe}(\text{bpy})(\text{CN})_4]^{18}$ ,  $\text{K}_2[\text{Fe}(\text{phen})(\text{CN})_4]^{18}$ ,  $\text{K}_4[\text{Ru}(\text{CN})_6]^{46}$ , and  $\text{K}_2[\text{Ru}(\text{bpy})(\text{CN})_4]^{19}$  were prepared using previously reported procedures. Tetrabutylammonium hydroxide (TBAOH) (Sigma Aldrich), bis(triphenylphosphine)iminium chloride (PPNCl) (Sigma Aldrich), 2,2'-bipyridine (bpy) (Sigma Aldrich), and 1,10-phenanthroline (phen) (Sigma Aldrich) were used as received. Triphenylborane (BPh<sub>3</sub>) (Sigma Aldrich) and tris(pentafluorophenyl)borane ( $\text{B}(\text{C}_6\text{F}_5)_3/\text{BCF}$ ) (TCI Chemicals) were purified from dry diethyl ether and hexanes, respectively. All solvents were dried, degassed, and stored over 3 Å molecular sieves. All boronation reactions were performed in a nitrogen-filled glove box. NMR spectra were collected on Varian 500 MHz and Bruker 400 MHz spectrometers ( $\delta$  in ppm, m: multiplet, s: singlet, d: doublet, t: triplet, pt: pseudo- triplet). <sup>19</sup>F NMR spectra were externally referenced to neat  $\text{CFCl}_3$ , and <sup>11</sup>B NMR were internally referenced to 15%  $\text{BF}_3 \cdot \text{Et}_2\text{O}$ . UV-visible spectra of complexes in MeCN were collected with a Varian Cary 50 Bio spectrophotometer. Infrared spectra were taken on a Thermo Scientific Nicolet iS5 FTIR spectrometer with an iD5 diamond ATR accessory. High resolution mass spectrometry was performed using a Waters LCT Premiere XE mass spectrometer (ESI-TOF, negative ion mode). Input files for density functional theory calculations are in Supporting Information.

## Electrochemistry

Electrochemical experiments were performed using a standard three electrode cell with a glassy carbon working electrode (3 mm diameter), a  $\text{Ag}^{+/\text{0}}$  in MeCN quasireference electrode, and a platinum counter electrode. Voltammograms were collected in a nitrogen-filled glove box on complexes in either MeCN or THF with 0.1–0.2 M TBAPF<sub>6</sub> as supporting electrolyte. A Gamry Reference 600 potentiostat was used for all room temperature voltammetry. All voltammograms were electronically compensated using positive-feedback iR-compensation for 85% of the  $R_{\text{u}}$ , as measured by potentiostatic electrochemical impedance spectroscopy.

## Transient Absorption Spectroscopy

Transient absorption measurements were collected using a pump-probe spectrometer (Helios, Ultrafast Systems) with detection in the ultraviolet region (800 nm/12,500  $\text{cm}^{-1}$  to 320 nm/31,250  $\text{cm}^{-1}$ ). This system delivers 5 mJ, 35 fs pulses at 800 nm with a 1 kHz repetition rate obtained from an amplified Ti:Al<sub>2</sub>O<sub>3</sub> laser (Coherent brand Astrella) with some output pumped into a commercial two-stage noncollinear optical parametric amplifier (Coherent OPerA Solo kHz). The pump wavelengths used in this study, 290 nm (34,500  $\text{cm}^{-1}$ ) and 700 nm (14,300  $\text{cm}^{-1}$ ), were obtained from the second and fourth harmonic of the signal beam. The probe beam was aligned with a computer-controlled program and focused on a 2 mm sapphire plate to generate a white light continuum. Some of the samples were also measured at longer wavelengths (approximately 390 nm); with no changes in TA spectra.

Samples were stirred by rotating a magnetic stirrer; insignificant sample degradation was observed over the time scale of the experiments as monitored by UV-vis absorption. The white probe light overlapped the pump beam in the sample holder, and the change in absorbance was measured with a charge-coupled detector. The pump pulse energy was 0.3 mW. The instrument response function for this setup was determined to be 90 fs. Transient absorption data were collected -10 ps before pump overlap. Over five scans, 500 steps were collected with an initial step of 0.01 ps, totaling 2500 points per spectrum. Scans were collected in an exponential stepping mode out to 1 ns. In the diimine complexes, a residual signal persisted following 290 nm excitation, corresponding to the solvated dimer anion of MeCN, which is in equilibrium with the solvated free electron, at time scales greater than 70 ps.<sup>47</sup> To eliminate confluence of this residual signal with measured kinetics, two component singular value decomposition and global analysis of transient spectra were performed according to literature procedures with the Surface Xplorer Data Analysis Program (Ultrafast Systems). Each spectrum was fit over the region 16,000–28,000  $\text{cm}^{-1}$  (**Fe-phen**) and 18,000–29,000  $\text{cm}^{-1}$  (**Fe-bpy-BPh<sub>3</sub>**, **Fe-phen-BPh<sub>3</sub>**, **Fe-bpy-BCF**, and **Fe-phen-BCF**) to a single exponential.<sup>48,49</sup>

## Synthesis

**(TBA)<sub>2</sub>[Fe(bpy)(CN-BPh<sub>3</sub>)<sub>4</sub>] (Fe-bpy-BPh<sub>3</sub>).** (TBA)<sub>2</sub>[Fe(bpy)(CN)<sub>4</sub>] (50.8 mg, 0.0634 mmol) dissolved in DCM was added to a solution of 5.1 equivalents of BPh<sub>3</sub> (78.6 mg, 0.325 mmol) in 5 mL of DCM. An immediate color change from dark green to orange was observed. The solution was refluxed overnight. The solution was allowed to cool to room temperature, and the solvent was removed *in vacuo* until a minimal

volume of DCM remained. 50 mL of hexanes were then added, and the solution was shaken. The solvent was decanted, and the precipitate was dissolved in minimal DCM. 50 mL of hexanes were again added. The solvent was decanted, and the precipitate was dried *in vacuo* overnight, yielding the product as an orange solid (0.0559 mmol, 88% yield). <sup>1</sup>H NMR (500 MHz, CD<sub>2</sub>Cl<sub>2</sub>)  $\delta$  <sup>1</sup>H NMR (500 MHz, Methylene Chloride-*d*<sub>2</sub>)  $\delta$  8.75 (d, *J* = 5.8, 2H), 7.72 – 7.54 (m, 16H), 7.05 – 6.91 (m, 50H), 2.59 – 2.45 (m, 16H), 1.29 – 1.12 (m, 32H), 0.87 (t, *J* = 7.0 Hz, 24H). <sup>11</sup>B NMR (128 MHz, CD<sub>3</sub>CN)  $\delta$  -3.62. TOF MS—ES-: m/z = 1,526.8151 (calc'd for (TBA)<sub>2</sub>[Fe(bpy)(CN-BPh<sub>3</sub>)<sub>4</sub>]<sup>2-</sup>: m/z = 1,526.8126). Selected IR data (ATR, 4,000–600  $\text{cm}^{-1}$ )  $\nu$  /  $\text{cm}^{-1}$ : 2,181, 2,145 (v<sub>CN</sub>). Elel. Anal. (for TBA salt) (%) found (calc'd): C, 80.09 (78.97); H, 7.97 (7.41); N, 6.33 (5.98).

**(TBA)<sub>2</sub>[Fe(bpy)(CN-B(C<sub>6</sub>F<sub>5</sub>)<sub>3</sub>)<sub>4</sub>] (Fe-bpy-BCF).**

(TBA)<sub>2</sub>[Fe(bpy)(CN)<sub>4</sub>] (111 mg, 0.139 mmol) was dissolved in 10 mL DCM and added to a solution of 5.0 equivalents of B(C<sub>6</sub>F<sub>5</sub>)<sub>3</sub> (358 mg, 0.699 mmol) in 15 mL of DCM. An immediate color change from dark green to yellow was observed. The solution was refluxed overnight, and the reaction vessel was allowed to cool to room temperature. The solvent was removed *in vacuo* until a minimal volume of DCM remained. 50 mL of hexanes were added, and the solvent was decanted. The resulting solid was then dissolved in minimal DCM, and 50 mL of hexanes was added. The solvent was decanted, and the precipitate was dried *in vacuo*, yielding the product as a yellow solid (0.133 mmol, 96% yield). <sup>1</sup>H NMR (400 MHz, CD<sub>3</sub>CN) 8.57 (m, 2H), 7.75 (m, 2H), 7.63 (m, 2H), 6.96 (m, 2H), 2.79 (m, 16H), 1.31 (m, 16H), 1.05 (m, 16H), 0.65 (m, 24H). <sup>11</sup>B NMR (128 MHz, CD<sub>3</sub>CN)  $\delta$  -14.44. <sup>19</sup>F NMR (376 MHz, CD<sub>3</sub>CN)  $\delta$  -134.64 (d, *J* = 21.9 Hz), -135.09 (d, *J* = 22.7 Hz), -162.55 (t, *J* = 18.9 Hz), -162.82 (t, *J* = 18.5 Hz), -167.80 (d, *J* = 21.4 Hz), -168.07 (d, *J* = 20.7 Hz). TOF MS—ES-: m/z = 1,181.9811 (calc'd for [Fe(bpy)(CN-B(C<sub>6</sub>F<sub>5</sub>)<sub>3</sub>)<sub>4</sub>]<sup>2-</sup>: m/z = 1,181.9810). Selected IR data (ATR, 4,000–600  $\text{cm}^{-1}$ )  $\nu$  /  $\text{cm}^{-1}$ : 2,207, 2,170 (v<sub>CN</sub>). Elel. Anal. (for TBA salt) (%) found (calc'd): C, 49.75 (49.38); H, 2.83 (2.76); N, 3.93 (3.70).

**(TBA)<sub>2</sub>[Fe(phen)(CN-BPh<sub>3</sub>)<sub>4</sub>] (Fe-phen-BPh<sub>3</sub>).** The general procedure used to prepare **Fe-bpy-BPh<sub>3</sub>** was followed, starting instead with (TBA)<sub>2</sub>[Fe(phen)(CN)<sub>4</sub>] to obtain the product as an orange powder (89% yield). <sup>1</sup>H NMR (500 MHz, CD<sub>2</sub>Cl<sub>2</sub>)  $\delta$  8.88 (dd, *J* = 5.8, 1.5 Hz, 2H), 8.09 (dd, *J* = 8.2, 1.3 Hz, 2H), 7.71 (s, 2H), 7.69 – 7.65 (m, 12H), 7.08 (dd, *J* = 8.2, 5.2 Hz, 2H), 7.04 (dd, *J* = 7.9, 6.6 Hz, 12H), 7.00 – 6.94 (m, 6H), 6.83 – 6.76 (m, 12H), 6.76 – 6.71 (m, 6H), 6.70 – 6.64 (m, 12H), 2.45 (t, 16H), 1.25 – 1.09 (m, 32H), 0.86 (t, *J* = 7.0 Hz, 24H). <sup>11</sup>B NMR (128 MHz, CD<sub>3</sub>CN)  $\delta$  -3.61. TOF MS—ES-: m/z = 1550.8112 (calc'd for (TBA)<sub>2</sub>[Fe(phen)(CN-BPh<sub>3</sub>)<sub>4</sub>]<sup>2-</sup>: m/z = 1,550.8126). Selected IR data (ATR, 4,000–600  $\text{cm}^{-1}$ )  $\nu$  /  $\text{cm}^{-1}$ : 2,182, 2,146 (v<sub>CN</sub>). Elel. Anal. (for TBA salt) (%) found (calc'd): C, 80.36 (79.07); H, 7.87 (7.88); N, 6.25 (5.82).

**(TBA)<sub>2</sub>[Fe(phen)(CN-B(C<sub>6</sub>F<sub>5</sub>)<sub>3</sub>)<sub>4</sub>] (Fe-phen-BCF).** The general procedure used to prepare **Fe-bpy-BCF** was followed, starting instead with (TBA)<sub>2</sub>[Fe(phen)(CN)<sub>4</sub>] to obtain the product as a yellow powder (94% yield). <sup>1</sup>H NMR (500 MHz, CD<sub>2</sub>Cl<sub>2</sub>)  $\delta$  9.14 (d, *J* = 5.2 Hz, 2H), 8.34 (dd, *J* = 8.2 Hz, 2H), 7.84 (s, 2H), 7.56 (dd, *J* = 8.1, 5.2 Hz, 2H), 3.08 (t, 16H, CH<sub>but</sub>, *J*<sub>HH</sub> = 8.2 Hz), 1.60 (pquint, 16H, CH<sub>but</sub>), 1.35 (psextet, 16H, CH<sub>but</sub>), 0.95 (t, 12H, CH<sub>but</sub>, *J*<sub>HH</sub> = 7.3 Hz). <sup>11</sup>B NMR (128 MHz, CD<sub>3</sub>CN)  $\delta$  -14.54. <sup>19</sup>F NMR (376 MHz, CD<sub>3</sub>CN)  $\delta$  -134.74 (d, *J* = 22.0 Hz), -135.53 (d, *J* = 22.5 Hz), -162.57 (t, *J* = 19.3 Hz), -162.79 (t, *J* = 19.1 Hz), -167.85 (pt, *J* = 19.8 Hz), -168.14 (pt,

$J = 19.3$  Hz). TOF MS—ES-: m/z = 1,193.9819 (calc'd for  $[\text{Fe}(\text{phen})(\text{CN-B}(\text{C}_6\text{F}_5)_3)_4]^{2-}$ : m/z = 1,193.9810). Selected IR data (ATR, 4,000–600  $\text{cm}^{-1}$ )  $\nu$  /  $\text{cm}^{-1}$ : 2206, 2169 ( $\nu_{\text{CN}}$ ). Elel. Anal. (for TBA salt) (%) found (calc'd): C, 50.17 (48.97); H, 2.81 (2.61); N, 3.90 (3.34).

**(TEA)<sub>2</sub>[Ru(bpy)(CN-BPh<sub>3</sub>)<sub>4</sub>] (Ru-bpy-BPh<sub>3</sub>).** The general procedure used to prepare Fe-bpy-BPh<sub>3</sub> was followed, starting instead with (TEA)<sub>2</sub>[Ru(bpy)(CN)<sub>4</sub>] to obtain the product as a yellow powder (79% yield). <sup>1</sup>H NMR (400 MHz, CD<sub>3</sub>CN)  $\delta$  8.90 (dd,  $J = 5.5, 1.6$  Hz, 2H), 8.21 (d,  $J = 8.2$  Hz, 2H), 7.95 (td,  $J = 7.9, 1.6$  Hz, 2H), 7.49 (dt,  $J = 7.8, 1.7$  Hz, 12H), 7.18 (ddd,  $J = 7.7, 5.5, 1.3$  Hz, 2H), 7.04 – 6.89 (m, 12H), 6.87 – 6.76 (m, 18H), 3.05 (q,  $J = 7.3$  Hz, 16H), 1.13 (tt,  $J = 1.9, 7.3$  Hz, 24H). <sup>11</sup>B NMR (128 MHz, CD<sub>3</sub>CN)  $\delta$  -5.19. TOF MS—ES-: m/z = 1,460.6587 (calc'd for (TEA)[Ru(bpy)(CN-BPh<sub>3</sub>)<sub>4</sub>]<sup>-</sup>: m/z = 1,460.6578). Selected IR data (ATR, 4,000–600  $\text{cm}^{-1}$ )  $\nu$  /  $\text{cm}^{-1}$ : 2,188, 2,140 ( $\nu_{\text{CN}}$ ). Elel. Anal. (for TEA salt) (%) found (calc'd): C, 39.57 (39.93); H, 2.22 (2.06); N, 6.81 (7.16).

**(TBA)<sub>2</sub>[Ru(bpy)(CN-B(C<sub>6</sub>F<sub>5</sub>)<sub>3</sub>)<sub>4</sub>] (Ru-bpy-BCF).** The general procedure used to prepare Fe-bpy-BCF was followed, starting instead with (TBA)<sub>2</sub>[Ru(bpy)(CN)<sub>4</sub>] to obtain the product as a colorless powder (99% yield). <sup>1</sup>H NMR (400 MHz, CD<sub>3</sub>CN)  $\delta$  8.79 (dd,  $J = 5.6, 1.5$  Hz, 2H), 8.16 (d,  $J = 8.2$  Hz, 2H), 7.99 (dd,  $J = 7.9, 1.6$  Hz, 2H), 7.34 (d,  $J = 7.4, 5.6$  Hz, 2H), 3.07 (t, 16H, CH<sub>but</sub>,  $J_{\text{HH}} = 8.6$  Hz), 1.59 (pquint, 16H, CH<sub>but</sub>), 1.34 (psextet, 16H, CH<sub>but</sub>), 0.95 (t, 12H, CH<sub>but</sub>,  $J_{\text{HH}} = 7.3$  Hz); <sup>11</sup>B NMR (128 MHz, CD<sub>2</sub>Cl<sub>2</sub>)  $\delta$  -14.19; <sup>19</sup>F NMR (376 MHz, CD<sub>2</sub>Cl<sub>2</sub>)  $\delta$  -134.28 (d,  $J = 16.0$  Hz), -134.57 (d,  $J = 15.4$  Hz), -162.19 (t,  $J = 20.2$  Hz), -162.60 (t,  $J = 20.0$  Hz), -167.25 (pt,  $J = 18.2$  Hz), -167.56 (pt,  $J = 18.3$  Hz). TOF MS—ES-: m/z = 1,204.9670 (calc'd for [Ru(bpy)(CN-B(C<sub>6</sub>F<sub>5</sub>)<sub>3</sub>)<sub>4</sub>]<sup>2-</sup>: m/z = 1204.9663). Selected IR data (ATR, 4,000–600  $\text{cm}^{-1}$ )  $\nu$  /  $\text{cm}^{-1}$ : 2,216, 2,168 ( $\nu_{\text{CN}}$ ). Elel. Anal. (for TBA salt) (%) found (calc'd): C, 48.97 (48.47); H, 2.79 (2.70); N, 3.87 (3.87).

**(PPN)<sub>2</sub>[Ru(fly)(CN)<sub>4</sub>] (Ru-fly).** K<sub>2</sub>Ru(fly)(CN)<sub>4</sub> was synthesized following a modified literature procedure.<sup>19</sup> To a boiling solution of K<sub>4</sub>Ru(CN)<sub>6</sub> (400 mg, 0.908 mmol) and fly (305 mg, 1.04 mmol) in 50 mL 1:1 methanol:water was added 400  $\mu\text{L}$  3.6 N H<sub>2</sub>SO<sub>4</sub> (pH = 4). The solution was refluxed for 24 h, over which time it slowly turned red; the solution was cooled to room temperature and neutralized. Excess fly was removed by filtration, and solvent also was removed. The remaining solid was purified by gel-filtration chromatography on a Sephadex G-15 column. Elution with water gave an orange band free of excess K<sub>4</sub>Ru(CN)<sub>6</sub>. The main fraction was dried under vacuum to give K<sub>2</sub>Ru(fly)(CN)<sub>4</sub> (30% yield). The cation was exchanged by precipitation from concentrated aqueous solution with a saturated solution of PPNCl (307 mg, 0.535 mmol) dissolved in 20 mL water. The resulting brick-red precipitate was collected by filtration and dried in a desiccator or under vacuum until it turned green (326 mg, 25% yield). Single crystals suitable for X-ray diffraction analysis were grown by slow evaporation from DCM solution. <sup>1</sup>H NMR (400 MHz, CD<sub>2</sub>Cl<sub>2</sub>): 8.97 (d,  $J = 8$  Hz, 2H, 6,6'-H), 8.14 (s, 2H, 3,3'-H), 7.71–7.65 (m, 24H, (PPN)), 7.54–7.46 (m, 36H, (PPN)), 7.44 (d,  $J = 8$  Hz, 2H, 5,5'-H). <sup>19</sup>F NMR (CD<sub>2</sub>Cl<sub>2</sub>):  $\delta$  -64.70. Selected IR data (ATR, 4,000–600  $\text{cm}^{-1}$ )  $\nu$  /  $\text{cm}^{-1}$ : 2,062, 2,090 ( $\nu_{\text{CN}}$ ). Elel. Anal. (for PPN salt) (%) found (calc'd): C, 67.13 (64.21); H, 4.23 (4.28); N, 7.12 (5.55).

**(PPN)<sub>2</sub>[Ru(fly)(CN-BCF)<sub>4</sub>] (Ru-fly-BCF).** (PPN)<sub>2</sub>Ru(fly)(CN)<sub>4</sub> (100. mg, 0.0637 mmol) and excess

B(C<sub>6</sub>F<sub>5</sub>)<sub>3</sub> (133 mg, 0.261 mmol) were dissolved in minimal DCM. The two solutions were combined, and an immediate color change from green to red to yellow was observed. The solution was refluxed for 1 h, then dried under vacuum. The resulting yellow solid was washed with 3 x 10 mL hexanes, then dried under vacuum. The resulting yellow solid was further purified by flash chromatography on silica gel (eluent gradient from 100% hexanes to 90% dichloromethane in hexanes), resulting in 131 mg yellow product (0.0362 mmol, 56% yield). Single crystals suitable for X-ray diffraction analysis were grown from a saturated ethanol solution at -25 °C. <sup>1</sup>H NMR (400 MHz, CD<sub>2</sub>Cl<sub>2</sub>):  $\delta$  9.22 (d,  $J = 4$  Hz, 2H, 6,6'-H), 8.29 (s, 2H, 3,3'-H), 7.65–7.59 (m, 14H, (PPN) + 5,5'-H), 7.51–7.40 (m, 48H, (PPN)). <sup>19</sup>F NMR (CD<sub>2</sub>Cl<sub>2</sub>):  $\delta$  -65.48 (s, 6F, CF<sub>3</sub>), -134.52 (dd, 12F, o-F), -134.99 (dd, 12F, o-F), -161.56 (t, 6F, p-F), -162.03 (t, 6F, p-F), -167.01 (td, 12F, m-F), -167.29 (td, 12F, m-F). <sup>11</sup>B NMR (CD<sub>2</sub>Cl<sub>2</sub>):  $\delta$  -14.05. Selected IR data (ATR, 4,000–600  $\text{cm}^{-1}$ )  $\nu$  /  $\text{cm}^{-1}$ : 2,171, 2,216 ( $\nu_{\text{CN}}$ ). Elel. Anal. (for PPN salt) (%) found (calc'd): C, 53.05 (51.69); H, 1.84 (2.09); N, 3.09 (2.76).

#### Collection and Refinement Details for (PPN)<sub>2</sub>[Fe(phen)(CN-BPh<sub>3</sub>)<sub>4</sub>]

Low-temperature diffraction data ( $\phi$ -and  $\omega$ -scans) were collected on a Bruker AXS D8 VENTURE KAPPA diffractometer coupled to a PHOTON II CPAD detector or Cu  $K_{\alpha}$  radiation ( $\lambda = 1.54178$  Å) from an  $I\mu\text{S}$  micro-source for the structure of compound (PPN)<sub>2</sub>[Fe(phen)(CN-BPh<sub>3</sub>)<sub>4</sub>]. The structure was solved by direct methods using SHELXS<sup>50</sup> and refined against  $F^2$  on all data by full-matrix least squares with SHELXL-2017<sup>51</sup> using established refinement techniques.<sup>52</sup> All non-hydrogen atoms were refined anisotropically. All hydrogen atoms were included in the model at geometrically calculated positions and refined using a riding model. The isotropic displacement parameters of all hydrogen atoms were fixed to 1.2 times the  $U$  value of the atoms they are linked to (1.5 times for methyl groups). All disordered atoms were refined with the help of similarity restraints on the 1,2- and 1,3-distances. (PPN)<sub>2</sub>[Fe(phen)(CN-B(C<sub>6</sub>F<sub>5</sub>)<sub>3</sub>)<sub>4</sub>] crystallized in the monoclinic space group  $C2c$  with half a molecule in the asymmetric unit along with half a molecule of dichloromethane. The dichloromethane molecule was located near a crystallographic symmetry element and disordered appropriately. One of the chlorine atoms was disordered over two additional positions.

#### Collection and Refinement Details for (PPN)<sub>2</sub>[Ru(fly)(CN-B(C<sub>6</sub>F<sub>5</sub>)<sub>3</sub>)<sub>4</sub>]

Low-temperature diffraction data ( $\phi$ -and  $\omega$ -scans) were collected on a Bruker AXS KAPPA APEX II diffractometer coupled to an PHOTON 100 CMOS detector with graphite monochromated Mo  $K_{\alpha}$  radiation ( $\lambda = 0.71073$  Å) for (PPN)<sub>2</sub>[Ru(fly)(CN-B(C<sub>6</sub>F<sub>5</sub>)<sub>3</sub>)<sub>4</sub>]. The structure was solved by direct methods using SHELXS<sup>50</sup> and refined against  $F^2$  on all data by full-matrix least squares with SHELXL-2017<sup>51</sup> using established refinement techniques.<sup>52</sup> All non-hydrogen atoms were refined anisotropically. All hydrogen atoms were included in the model at geometrically calculated positions and refined using a riding model. The isotropic displacement parameters of all hydrogen atoms were fixed to 1.2 times the  $U$  value of the atoms they are linked to (1.5 times for methyl groups). All disordered atoms were refined with the help of similarity restraints on the 1,2- and 1,3-distances and displacement parameters as well as enhanced rigid bond restraints for anisotropic displacement parameters. (PPN)<sub>2</sub>[Ru(fly)(CN-B(C<sub>6</sub>F<sub>5</sub>)<sub>3</sub>)<sub>4</sub>] crystallized in the triclinic space group  $P-1$  with one molecule in the asymmetric unit along with half a molecule of ethanol. One phenyl

and two pentafluorophenyl groups were disordered over two positions. All disordered aromatic rings were restrained to be flat. The ethanol was located near a crystallographic inversion center and disordered over six positions, three of which are pairwise related to the other three by the inversion center. The O-C and C-C distances in the disordered ethanol were restrained to be 1.43(2) Å and 1.54(2) Å respectively.

#### Collection and Refinement Details for $(PPN)_2[Ru(fly)(CN)_4]$

A crystal was mounted on a polyimide MiTeGen loop with STP Oil Treatment and placed under a nitrogen stream. Low temperature (100K) X-ray data were collected with a Bruker AXS D8 VENTURE KAPPA diffractometer running at 50 kV and 1mA ( $Cu K_{\alpha} = 1.54178$  Å; PHOTON II CPAD detector and Helios focusing multilayer mirror optics). All diffractometer manipulations, including data collection, integration, and scaling were carried out using the Bruker APEX3 software. An absorption correction was applied using SADABS. The space group was determined, and the structure solved by intrinsic phasing using XT. Refinement was full-matrix least squares on  $F^2$  using XL. All non-hydrogen atoms were refined using anisotropic displacement parameters. Hydrogen atoms were placed in idealized positions and the coordinates refined. The isotropic displacement parameters of all hydrogen atoms were fixed at 1.2 times the  $U_{eq}$  value of the bonded atom.  $(PPN)_2[Ru(fly)(CN)_4]$  crystallized in the triclinic space group P-1 (# 2) with one ruthenium anion, two PPN cations, and 2.2  $CH_2Cl_2$  in the asymmetric unit.

#### Collection and Refinement Details for $(TBA)(Ph_4As)[Fe(phen)(CN-B(C_6F_5)_3)_4]$

A crystal was mounted on a polyimide MiTeGen loop with STP Oil Treatment and placed under a nitrogen stream. Low temperature (100K) X-ray data were collected with a Bruker AXS D8 VENTURE KAPPA diffractometer running at 50 kV and 1mA ( $Cu K_{\alpha} = 1.54178$  Å; PHOTON II CPAD detector and Helios focusing multilayer mirror optics). All diffractometer manipulations, including data collection, integration, and scaling were carried out using the Bruker APEX3 software. An absorption correction was applied using SADABS. The space group was determined, and the structure was solved by intrinsic phasing using XT. Refinement was full-matrix least squares on  $F^2$  using XL. All non-hydrogen atoms were refined using anisotropic displacement parameters. Hydrogen atoms were placed in idealized positions and the coordinates refined. The isotropic displacement parameters of all hydrogen atoms were fixed at 1.2 times the  $U_{eq}$  value of the bonded atom.  $(TBA)(Ph_4As)[Fe(phen)(CN-B(C_6F_5)_3)_4]$  crystallized in the triclinic space group P-1 (# 2) with one Fe anion, one Ph<sub>4</sub>As cation, and one TBA cation in the asymmetric unit.

### ASSOCIATED CONTENT

The Supporting Information is available free of charge on the ACS Publications website at DOI: XXXX.

Materials and methods, synthetic protocols, additional UV-visible and transient absorption spectra, additional voltammetry, X-ray crystallographic data, and DFT/CASSCF+NEVPT2 input files.

### AUTHOR INFORMATION

#### Corresponding Authors

\*E-mail: [hbgray@caltech.edu](mailto:hbgray@caltech.edu)

\*E-mail: [bmenicho@caltech.edu](mailto:bmenicho@caltech.edu)

#### Funding Sources

This work was supported by the National Science Foundation (CHE-1763429). Additional funding was provided by an Arthur A. Noyes SURF Fellowship (D. X. N.) and the Beckman Institute Laser Resource Center and the Arnold and Mabel Beckman Foundation.

### ACKNOWLEDGMENT

We thank Jay Winkler for help in interpretation of transient absorption spectra. Larry Henling and Mike Takase provided invaluable assistance in collection and refinement of X-ray crystal structures. We acknowledge the X-Ray Crystallography Facility in the Beckman Institute at Caltech and the Dow Next Generation Instrumentation Grant for X-ray structure collection. We thank David van der Velde for assistance in NMR interpretation. Calculations were made on the Caltech High Performance Cluster, partially supported by a grant from the Gordon and Betty Moore Foundation.

### REFERENCES

- (1) Garcia Posse, M. E.; Katz, N. E.; Baraldo, L. M.; Polonuer, D. D.; Colombano, C. G.; Olabe, J. A. Comparative Bonding and Photophysical Properties of 2,2'-Bipyridine and 2,2'-Bipyrazine in Tetracyano Complexes Containing Ruthenium and Osmium. *Inorg. Chem.* **1995**, *34*, 1830–1835.
- (2) Winkler, J. R.; Creutz, C.; Sutin, N. Solvent Tuning of the Excited-State Properties of (2,2'-Bipyridine)Tetracyanoferrocene(II): Direct Observation of a Metal-to-Ligand Charge-Transfer Excited State of Iron(II). *J. Am. Chem. Soc.* **1987**, *109*, 3470–3471.
- (3) Chan, K.-C.; Cheng, S.-C.; Lo, L. T.-L.; Yiu, S.-M.; Ko, C.-C. Luminescent Charge-Neutral Copper(I) Phenanthroline Complexes with Isocyanoborate Ligand: Luminescent Charge-Neutral Copper(I) Phenanthroline Complexes with Isocyanoborate Ligand. *Eur. J. Inorg. Chem.* **2018**, *2018*, 897–903.
- (4) Chan, K.-C.; Chu, W.-K.; Yiu, S.-M.; Ko, C.-C. Synthesis, Characterization, Photophysics and Electrochemical Study of Luminescent Iridium(III) Complexes with Isocyanoborate Ligands. *Dalton Trans.* **2015**, *44*, 15135–15144.
- (5) Chu, W.-K.; Ko, C.-C.; Chan, K.-C.; Yiu, S.-M.; Wong, F.-L.; Lee, C.-S.; Roy, V. A. L. A Simple Design for Strongly Emissive Sky-Blue Phosphorescent Neutral Rhenium Complexes: Synthesis, Photophysics, and Electroluminescent Devices. *Chem. Mater.* **2014**, *26*, 2544–2550.
- (6) Ahrens, M. J.; Bertin, P. A.; Gaustad, A. G.; Georganopoulos, D.; Wunder, M.; Blackburn, G. F.; Gray, H. B.; Meade, T. J. Spectroscopic and Redox Properties of Amine-Functionalized  $K_2[Os^{II}(Bpy)(CN)_4]$  Complexes. *Dalton Trans.* **2011**, *40*, 1732.
- (7) Chu, W.-K.; Yiu, S.-M.; Ko, C.-C. Neutral Luminescent Bis(Bipyridyl) Osmium(II) Complexes with Improved Phosphorescent Properties. *Organometallics* **2014**, *33*, 6771–6777.
- (8) Evju, J. K.; Mann, K. R. Synthesis and Spectroscopic Investigations of a Crystalline Humidity Sensor: Bis(Triphenylphosphine)Iminium 2,2'-Bipyridyltetracyanoruthenate. *Chem. Mater.* **1999**, *11*, 1425–1433.
- (9) Chu, W.-K.; Wei, X.-G.; Yiu, S.-M.; Ko, C.-C.; Lau, K.-C. Strongly Phosphorescent Neutral Rhenium(I) Isocyanoborate Complexes: Synthesis, Characterization, and Photophysical, Electrochemical, and Computational Studies. *Chem. - Eur. J.* **2015**, *21*, 2603–2612.
- (10) Bignozzi, C. A.; Chiorboli, C.; Indelli, M. T.; Rampi Scandola, M. A.; Varani, G.; Scandola, F. Simple Poly(Pyridine)Ruthenium(II) Photosensitizer: (2,2'-Bipyridine)Tetracyanoruthenate(II). *J. Am. Chem. Soc.* **1986**, *108*, 7872–7873.

(11) Shriner, D. F.; Posner, J. Bridge Addition Compounds. III. The Influence of Boron-Containing Lewis Acids on Electronic Spectra, Vibrational Spectra, and Oxidation Potentials of Some Iron-Cyanide Complexes. *J. Am. Chem. Soc.* **1966**, *88*, 1672–1677.

(12) Shriner, D. F.; Swanson, B. Nature of the Donor-Acceptor Interaction in Boron Trihalide Complexes. Vibrational Spectra and Vibrational Analysis of Acetonitrile-Boron Trichloride and Acetonitrile-Boron Tribromide. *Inorg. Chem.* **1971**, *10*, 1354–1365.

(13) Shriner, D. F.; Shriner, S. A.; Anderson, S. E. Ligand Field Strength of the Nitrogen End of Cyanide and Structures of Cubic Cyanide Polymers. *Inorg. Chem.* **1965**, *4*, 725–730.

(14) McNicholas, B. J.; Grubbs, R. H.; Winkler, J. R.; Gray, H. B.; Despagne-Ayoub, E. Tuning the Formal Potential of Ferrocyanide over a 2.1 V Range. *Chem. Sci.* **2019**, *10*, 3623–3626.

(15) Indelli, M. Teresa.; Bignozzi, C. Alberto.; Marconi, Anna.; Scandola, Franco. Ruthenium(II) 2,2'-Bipyridine Complexes Containing Methyl Isocyanoide Ligands. Extreme Effects of Nonchromophoric Ligands on Excited-State Properties. *J. Am. Chem. Soc.* **1988**, *110*, 7381–7386.

(16) Bignozzi, C. A.; Indelli, M. T.; Scandola, F. Bis(2,2'-Bipyridine)Ruthenium(II)-Hexacyanochromate(III) Chromophore-Luminophore Complexes. Intramolecular Energy Transfer, Excited-State Intervalence Transfer, and Doublet-Doublet Annihilation. *J. Am. Chem. Soc.* **1989**, *111*, 5192–5198.

(17) Indelli, M. T.; Ghirotti, M.; Prodi, A.; Chiorboli, C.; Scandola, F.; McClenaghan, N. D.; Puntoriero, F.; Campagna, S. Solvent Switching of Intramolecular Energy Transfer in Bichromophoric Systems: Photophysics of (2,2'-Bipyridine)Tetracyanoruthenate(II)/Pyrenyl Complexes. *Inorg. Chem.* **2003**, *42*, 5489–5497.

(18) Schilt, A. A. Mixed Ligand Complexes of Iron(II) and (III) with Cyanide and Aromatic Di-Imines. *J. Am. Chem. Soc.* **1960**, *82*, 3000–3005.

(19) Jiwan, J. L. H.; Wegewijs, B.; Indelli, M. T.; Scandola, F.; Braslavsky, S. E. Volume Changes Associated with Intramolecular Electron Transfer during MLCT State Formation. Time-Resolved Optoacoustic Studies of Ruthenium Cyano Complexes. *Recl. Trav. Chim. Pays-Bas-J. R. Neth. Chem. Soc.* **1995**, *114*, 542–548.

(20) Kjær, K. S.; Kunnus, K.; Harlang, T. C. B.; Van Driel, T. B.; Ledbetter, K.; Hartsock, R. W.; Reinhard, M. E.; Koroidov, S.; Li, L.; Laursen, M. G.; Biasin, E.; Hansen, F. B.; Vester, P.; Christensen, M.; Haldrup, K.; Nielsen, M. M.; Chabera, P.; Liu, Y.; Tatsuno, H.; Timm, C.; Uhlig, J.; Sundström, V.; Németh, Z.; Szemes, D. S.; Bajnóczi, É.; Vankó, G.; Alonso-Mori, R.; Glownia, J. M.; Nelson, S.; Sikorski, M.; Sokaras, D.; Lemke, H. T.; Canton, S. E.; Wärnmark, K.; Persson, P.; Cordones, A. A.; Gaffney, K. J. Solvent Control of Charge Transfer Excited State Relaxation Pathways in  $[\text{Fe}(2,2'\text{-Bipyridine})(\text{CN})_4]^{2-}$ . *Phys. Chem. Chem. Phys.* **2018**, *20*, 4238–4249.

(21) Toma, H.E., Takasugi, M.S. Spectroscopic studies of preferential and asymmetric solvation in substituted cyanoiron(II) complexes. *J. Solution Chem.* **1983**, *12*, 547–561.

(22) Timpson, C. J.; Bignozzi, C. A.; Sullivan, B. P.; Kober, E. M.; Meyer, T. J. Influence of Solvent on the Spectroscopic Properties of Cyano Complexes of Ruthenium(II). *J. Phys. Chem.* **1996**, *100*, 2915–2925. <https://doi.org/10.1021/jp953179m>.

(23) Shriner D.F. (1966) The ambident nature of cyanide. In: *Structure And Bonding. Structure and Bonding*, vol 1. Springer, Berlin, Heidelberg

(24) Ward, M. D.  $[\text{Ru}(\text{Bipy})(\text{CN})_4]^{2-}$  and Its Derivatives: Photophysical Properties and Its Use in Photoactive Supramolecular Assemblies. *Coord. Chem. Rev.* **2006**, *250*, 3128–3141.

(25) Ngo, D.; Del Ciello, S. A.; McNicholas, B. J.; Sanders, B. C.; Fajardo Jr., J.; Gray, H. B.; Winkler, J. R. Cyano-Ambivalence: Spectroscopy and Photophysics of  $[\text{Ru}(\text{diimine})(\text{CN}-\text{BR}_3)_4]^{2-}$  *Polyhedron* **2020**, submitted for publication.

(26) Gutmann, V.; Gritzner, G.; Danksagmoller, K. Solvent Effects on the Redox Potential of Hexacyanoferrate(III)-Hexacyanoferrate(II) *Inorganica Chim. Acta* **1976**, *17*, 81–86.

(27) Zhou, Y.; Xiao, H.-P.; Kang, L.-C.; Zuo, J.-L.; Li, C.-H.; You, X.-Z. Synthesis and Characterization of Neutral Iron(II) and Ruthenium(II) Complexes with the Isocyano-triphenylborate Ligand. *Dalton Trans.* **2009**, *46*, 10256.

(28) Espinoza, E. M.; Clark, J. A.; Soliman, J.; Derr, J. B.; Morales, M.; Vullev, V. I. Practical Aspects of Cyclic Voltammetry: How to Estimate Reduction Potentials When Irreversibility Prevails. *J. Electrochem. Soc.* **2019**, *166*, H3175–H3187.

(29) Creutz, C. Bipyridine Radical Ions *Comment. Inorg. Chem.* **1982**, *1*, 293–311.

(30) Kato, T.; Shida, T. Electronic Structures of Ion Radicals of Nitrogen-Heteroaromatic Hydrocarbons as Studied by ESR and Optical Spectroscopy. *J. Am. Chem. Soc.* **1979**, *101*, 6869–6876.

(31) Liu, Y.; Kjaer, K. S.; Fredin, L. A.; Chábera, P.; Harlang, T.; Canton, S. E.; Lidin, S.; Zhang, J.; Lomoth, R.; Bergquist, K.-E.; Persson, P.; Wärnmark, K.; Sundström, V. A Heteroleptic Ferrous Complex with Mesoionic Bis(1,2,3-Triazol-5-Ylidene) Ligands: Taming the MLCT Excited State of Iron(II). *Chem. - Eur. J.* **2015**, *21*, 3628–3639.

(32) Zhang, W.; Kjær, K. S.; Alonso-Mori, R.; Bergmann, U.; Chollet, M.; Fredin, L. A.; Hadt, R. G.; Hartsock, R. W.; Harlang, T.; Kroll, T.; Kubíček, K.; Lemke, H. T.; Liang, H. W.; Liu, Y.; Nielsen, M. M.; Persson, P.; Robinson, J. S.; Solomon, E. I.; Sun, Z.; Sokaras, D.; van Driel, T. B.; Weng, T.-C.; Zhu, D.; Wärnmark, K.; Sundström, V.; Gaffney, K. J. Manipulating Charge Transfer Excited State Relaxation and Spin Crossover in Iron Coordination Complexes with Ligand Substitution. *Chem. Sci.* **2017**, *8*, 515–523.

(33) Kolling, O. W. Comparisons between Hydrogen Bond Donor-Acceptor Parameters and Solvatochromic Red Shifts. *Anal. Chem.* **1978**, *50*, 212–215.

(34) Pierloot, K.; Van Praet, E.; Vanquickenborne, L. G.; Roos, B. O. Systematic Ab Initio Study of the Ligand Field Spectra of Hexacyanometalate Complexes. *J. Phys. Chem.* **1993**, *97*, 12220–12228.

(35) Hahn, A. W.; Van Kuiken, B. E.; Chilkuri, V. G.; Levin, N.; Bill, E.; Weyhermüller, T.; Nicolaou, A.; Miyawaki, J.; Harada, Y.; DeBeer, S. Probing the Valence Electronic Structure of Low-Spin Ferrous and Ferric Complexes Using 2p3d Resonant Inelastic X-Ray Scattering (RIXS). *Inorg. Chem.* **2018**, *57*, 9515–9530.

(36) Formiga, A. L. B.; Vancoillie, S.; Pierloot, K. Electronic Spectra of *N*-Heterocyclic Pentacyanoferrate(II) Complexes in Different Solvents, Studied by Multiconfigurational Perturbation Theory. *Inorg. Chem.* **2013**, *52*, 10653–10663.

(37) Jakubczyk, M.; Adamczyk-Woźniak, A.; Sporzyński, A. Acceptor Number of Organoboron Molecules - Quantitative Determination of Lewis Acidity. In *Molecular Receptors*; East Publisher House: Donetsk, 2011; pp 53–68.

(38) Neese, F. The ORCA Program System. Wiley Interdisciplinary Reviews: Computational Molecular Science **2012**, *2*, 73–78.

(39) Mayer, U., Gutmann, V.; Gerger, W. The acceptor number — A quantitative empirical parameter for the electrophilic properties of solvents. *Monatshefte für Chemie* **1975**, *106*, 1235–1257.

(40) Bard, A. J.; Faulkner, L. R. *Electrochemical Methods*; Wiley: New York, 2000

(41) Nicholson, R. S. Semiempirical Procedure for Measuring with Stationary Electrode Polarography Rates of Chemical Reactions Involving the Product of Electron Transfer. *Anal. Chem.* **1966**, *38*, *10*, 1406.

(42) Roffia, S.; Ciano, M. Electrochemical behaviour of dicyanobis(2,2'-bipyridine) ruthenium(II) and dicyanobis(1,10-phenanthroline) ruthenium(II) complexes. *J. Electroanal. Chem.* **1977**, *77*, 349–359.

(43) Prier, C. K.; Rankic, D. A.; MacMillan, D. W. C. Visible Light Photoredox Catalysis with Transition Metal Complexes: Applications in Organic Synthesis. *Chem. Rev.* **2013**, *113*, 5322–5363.

(44) Pavlishchuk, V. V.; Addison, A. W. Conversion Constants for Redox Potentials Measured versus Different Reference Electrodes in Acetonitrile Solutions at 25°C. *Inorganica Chim. Acta* **2000**, *298*, 97–102.

(45) Potash, R. A.; McKone, J. R.; Conte, S.; Abruña, H. D. On the Benefits of a Symmetric Redox Flow Battery. *J. Electrochem. Soc.* **2016**, *163*, A338–A344.

(46) Krause, R. A.; Violette, C. An Improved Synthesis of Potassium Hexacyanoruthenate(II). *Inorganica Chim. Acta* **1986**, *113*, 161–162.

(47) Doan, S. C.; Schwartz, B. J. Ultrafast Studies of Excess Electrons in Liquid Acetonitrile: Revisiting the Solvated Electron/Solvent Dimer Anion Equilibrium. *J. Phys. Chem. B* **2013**, *117*, 4216–4221.

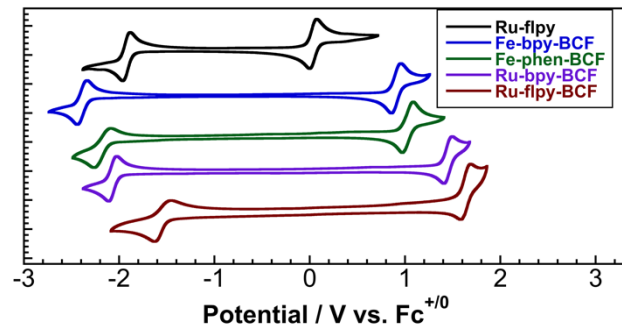
(48) *Surface Xplorer*; Ultrafast Systems LLC: Sarasota, FL, 2012.

(49) Gawelda, W.; Cannizzo, A.; Pham, V.-T.; van Mourik, F.; Bressler, C.; Chergui, M. Ultrafast Nonadiabatic Dynamics of  $[\text{Fe}^{\text{II}}(\text{Bpy})_3]^{2+}$  in Solution. *J. Am. Chem. Soc.* **2007**, *129*, 8199–8206.

(50) Sheldrick, G. M. Phase annealing in SHELX-90: direct methods for larger structures. *Acta Crystallogr.* **1990**, *A46*, 467–473.

(51) Sheldrick, G. M. Crystal structure refinement with SHELXL. *Acta Crystallogr.* **2015**, *C71*, 3–8.

(52) Müller, P. Practical suggestions for better crystal structures. *Crystallogr. Rev.* **2009**, *15*, 57–83.



Voltammetry of parent and boronated  $[M(\text{diimine})(\text{CN})_4]^{2-}$  complexes, demonstrating large formal potential separations between ligand-centered reduction and metal-centered oxidation.

---